ORIGINAL ARTICLE

Study of CNC skew rolling of hollow rail axles with a mandrel

Tomasz Bulzak[1] [ORCID] **· Zbigniew Pater[1] · Janusz Tomczak[1] · Łukasz Wójcik[1]**

Abstract

The manuscript presents a new manufacturing technology for the production of hollow railway axle forgings. The manufacturing technology analyzed is based on three-roll skew rolling (TRSR) using a computer numerically controlled (CNC) rolling mill. The study focused on comparing the rolling capability of hollow products without and with a mandrel calibrating the hole of the forging. The influence of tube billet size on the rolling process was also analyzed. FE analysis and experimental studies were carried out. An analysis of the accuracy of the internal hole of the forging depending on the adopted parameters of the rolling process was carried out. Based on numerical simulations, the state of strain and the flow pattern of the material and temperature distribution during rolling were determined. The force parameters of the rolling process of hollow forgings were also analyzed. Based on the research, a two-stage rolling technology for rolling hollow railway axle forgings was proposed. The results obtained indicate the suitability of using a calibrating mandrel to improve hole accuracy in hollow forgings rolled from a tubular billet. The gap c between the bore diameter of the forging and the diameter of the mandrel was measured. Increasing the tubular billet dimensions from $\varnothing42.4 \times 10$ mm to $\varnothing48.3 \times 12.5$ mm reduced the gap c by 49.8%. Rolling the billet $\varnothing51 \times 14.2$ mm in two passes compared to rolling in one pass reduced the gap c by 45.5%.

Keywords Hollow axle · Railway axle · Mandrel · Skew rolling

1 Introduction

The term high-speed rail is used to describe railway lines on which a travelling speed of 200 km/h or more can be achieved [1]. The term high-speed rail refers not only to railway lines, but also to rolling stock [2]. The adaptation of rolling stock to high speed increases the demand for high-speed railway wheelsets and new generation frames manufactured by laser-arc hybrid welding (LAHW) process [3]. The railway wheelset is the most important technical component of a railway vehicle and ensures that the vehicle interacts correctly with the rails [4]. A railway wheelset consists of railway wheels (overall wheel or split wheel) and railway axles (passenger axles, freight axles, and locomotive axles) [5]. The railway axle is one of the most sensitive components, as it is responsible for transferring the entire weight of the rail vehicle to the wheels [6]. During the service life of a rail vehicle, its axles are exposed to complex static and dynamic loads, particularly at its ends [7]. Rail axles should also meet the highest fatigue strength requirements [8], as fatigue is responsible for the majority of rail axle failures [9]. The continuous development of high-speed railways and the need to maintain rolling stock in serviceable condition necessitates the continuous production of railway axles and the search for more efficient manufacturing technologies for these components [10]. High-speed railways also need solutions to reduce the weight of structures to increase performance with lower energy consumption costs [11]. One such solution is definitely the use of lighter components such as hollow railway axles [12]. The advantage of hollow axles is that, with less weight, the axles can to provide a bending strength comparable to that of solid axles [13].

Currently, railway axles are manufactured from ingots by forging or rolling technologies as solid products [14].

✉ Tomasz Bulzak
  t.bulzak@pollub.pl

  Zbigniew Pater
  z.pater@pollub.pl

  Janusz Tomczak
  j.tomczak@pollub.pl

  Łukasz Wójcik
  l.wojcik@pollub.pl

[1] Lublin University of Technology, Nadbystrzycka 36, 20-618 Lublin, Poland

Forging on swaging machines, presses and hammers is used for manufacturing rail axles [15]. The advantages of open forging are the possibility of forming products of large sizes and large weights; on the other hand, the process is limited to forming products of non-complex shape [16]. Rolling processes are used sporadically despite their many advantages, such as high productivity, which is much higher than forging processes. To obtain a hollow axle, a hole is drilled in a solid axle forging. By drilling a hole, an axle with a uniform inner diameter can be obtained, which is required for strength reasons. The dimensions of a standard railway axle necessitate the use of deep drilling technology to produce the hole [17]. Deep drilling the railway axle hole leads to longer production times, generates material losses, creates problems with the removal of chips and heat generated during drilling, and requires the use of specialized machinery and tools [18].

Research work is also being carried out on lightweight composite railway axles [19]. The idea behind composite axles is to significantly reduce their weight, which can be reduced by 63% compared to a typical steel hollow railway axle [20]. A composite axle is constructed from a steel hollow flange, on which the wheels and bearings are mounted, while the rest of the axle is constructed from a composite tube (carbon fiber/epoxy resin) [21]. The use of composite railway axles is undoubtedly a very innovative solution in the railway industry. Nevertheless, it is still at the research stage and the possibility of its implementation will certainly depend on the production costs of this type of axle [22].

Technologies using hollow billets such as tubes or thick-walled bushings can also be used to produce hollow axles. For the production of hollow axles from hollow billets, various rolling methods can be used. One such method is cross wedge rolling (CWR). The concept of rolling a hollow axis from a tubular billet with three rollers was presented by Pater et al. [23]. Numerical simulations carried out by these authors have shown that free rolling (without mandrel) produces a hollow axle, the inner hole of which has different diameters along the length of the axle. This solution is not very advantageous because alignment of the axle bore diameter results in a dangerous reduction of the axle wall thickness in the area of the extreme steps. The use of a calibrating mandrel in this case requires the use of a mandrel slightly longer than the axle length. This solution can cause problems with later removal of the mandrel when the mandrel is clamped over the entire length of the axle, which exceeds 2 m in length [24]. Also, the use of three-roll mills alone for CWR technology can be problematic due to the lack of availability of such solutions on the market. The use of two-tool (roll or flat) rolling mills is also not advantageous, due to the high ovalization of the tubular billet during rolling. Billet ovalization makes it difficult to

control and stabilize the rolling process, as described, e.g., in a study published by Shen et al. [25].

A new rolling method that enables the rolling of hollow axles from tubular billets is the skew rolling process in CNC rolling mills. Research into this technology was carried out by Shu et al. [26]. The results obtained confirmed the possibility of rolling hollow axles with this technology. Nevertheless, free (without mandrel) skew rolling is also characterized by the fact that the hollow axle has a non-homogeneous internal bore in terms of diameter. An advantageous feature of the skew rolling process is the possibility to refine the grain size of the material from which the axle is made. The CNC free skew rolling process using three and four rollers was also analyzed by Pater [27]. The results of numerical simulations indicated that the four-roller rolling process has a greater reduction in axle wall thickness compared to a three-roller rolled axle. On the other hand, the four-roller rolling process reduces the energy required to roll the axle by approximately 20% compared to the three-roller rolling process.

From the information presented, it can be concluded that a major problem in the manufacture of hollow axles using rolling technologies is the non-uniformity of the diameter dimension of the axle bore. This problem can be attempted and solved using a mandrel to calibrate the hollow axle bore. A review of the literature has shown that, in the case of CWR technology, the use of a mandrel is not technologically justified. In the case of skew rolling, the use of a mandrel is technologically more correct. This is because the skew rolling process allows incremental forming of the axle, which allows the calibration of the hole by the mandrel to take place only in a small rolling zone. As a result, the mandrel is clamped over a much shorter length than the length of the entire axle, eliminating permanent locking of the mandrel in the rolled-off hollow axle forging. In summary, the main objective of this work is to investigate whether the use of a calibrating mandrel in the rolling zone allows hollow railway axles to be shaped with a relatively uniform bore diameter dimension.

A novelty of the ongoing research is the use of mandrel in the production of hollow products by skew rolling. Previous attempts to produce hollow products using this method were carried out without the use of a mandrel. To achieve this objective, an FE analysis of the manufacture of railway axles using CNC skew rolling with mandrel from billets of different sizes was carried out. The results of the FE analysis were verified in experimental studies. Based on the analysis, a new scheme of skew rolling with mandrel was developed and successfully verified. Regarding previous work carried out by Shu et al. [26] and Pater [27], this article deals with the problem of using a mandrel to calibrate the bore of a forging. In addition, the influence of billet size on the skew rolling process is discussed.

2 Objective and research methodology

The aim of the research carried out was to determine the possibility of rolling hollow railway axles. The adopted research objective will be achieved when the inner hole of the railway axle forging has as constant a diameter as possible. Based on the formulated research objective, it was assumed that the subject of the study would be the oblique rolling process of a hollow railway axle forging with a mandrel, without a mandrel and for various initial dimensions of the tubular billet. A schematic of the adopted concept for the skew rolling of a hollow axle forging with a mandrel is shown in Fig. 1. The selection of tube billets assumed that the diameter of the tube bore in each of the analyzed cases was at a similar level. This approach made it possible to assess the possibility of reducing the inner diameter of the tube to the mandrel size, depending on the degree of deformation of the outer diameter. Commercial tubes with the following outside diameter x wall thickness

dimensions were used in the study: $\varnothing 42.4 \times 10$ mm, $\varnothing 48.3 \times 12.5$ mm and $\varnothing 51 \times 14.2$ mm.

Investigations into the process of rolling rail axles on a mandrel were carried out using the finite element method FEA and experimental tests under laboratory conditions. The dimensions of the hollow axle forging selected for testing are illustrated in Fig. 2. The numerical model built in the FEM software was identical to the scheme shown in Fig. 1. In the tests, the tubular billet was assumed to be deformable, while the other tools were rigid objects. FEA studies were carried out in Simufact Forming software. The tubular billets were divided using four-node hexahedral elements with an average size of 1.75 mm. Depending on the size of the tubular billet, the number of finite elements was: for the tube $\varnothing 42.4 \times 10$ mm there were 63,000 finite elements, for the tube $\varnothing 48.3 \times 12.5$ mm there were 65,000 finite elements and for $\varnothing 51 \times 14.2$ mm there were 68,700 finite elements. In the rolling process analyzed, large plastic strains occur, resulting in excessive distortion of the finite element mesh. To eliminate excessive distortion of the finite element mesh, remeshing was considered during the
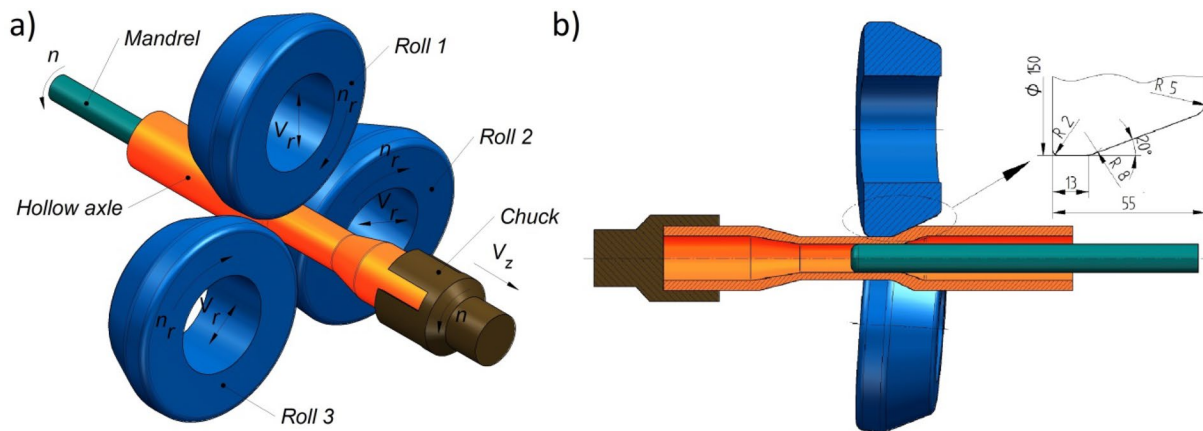

Fig. 1 Concept of skew rolling on a mandrel of hollow railway axles: **a** isometric view, **b** axial section view
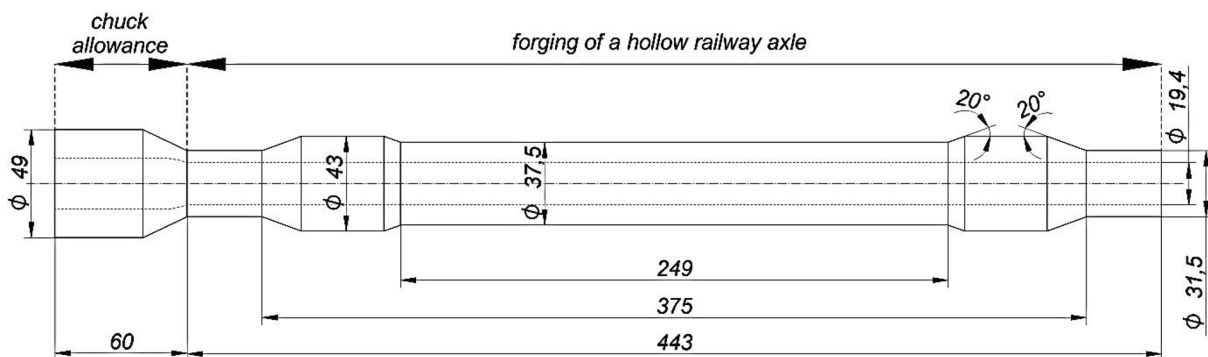

Fig. 2 A hollow forging of a railway axle in the hot state on a scale of 1:5

calculation, which was activated each time the strain value increased by 0.4. The seamless tubes used in the tests were made of S355J grade steel. Steel S355J used in the study is a non-alloy structural steel with good strength properties. The ultimate tensile strength of S355J steel ranges from 470–630 MPa. The minimum yield strength is 355 MPa. Its properties are on a par with EA1N steel, from which railway axles are manufactured. There is a large availability of seamless tubes made from S355J steel on the market, unlike, for example, typical railway steel. S355J steel also has good weldability. S355J steel can be machined, forged and rolled. S355J steel is widely used in construction, metallurgy, heavy and transport engineering, engineering, power generation and bridge construction [28]. The flow stress for S355J steel is expressed by the following equation:

$$
\sigma_f = 2478.72 \times e^{-0.00298T} \times \varepsilon^{(-0.000423T+0.3658)} \\
\times e^{\frac{-7.508e-05T+0.0315}{\varepsilon}} \times \dot{\varepsilon}^{0.00026T-0.137},
$$

(1)

where σ_f is the flow stress, ε is the effective strain, $\dot{\varepsilon}$ is the strain rate, T is the temperature. The hollow billets were heated to 1180 °C before the rolling process. The tool temperature, on the other hand, was fixed at 100 °C for the rollers and chuck, while the mandrel temperature was assumed to be 500 °C. The forming rollers performed rotary motion at a constant velocity n_r of 60 rpm. The trajectory of movement of the forming rollers, determined by the velocity V_r, and the chuck, determined by the velocity V_z, is shown in Fig. 3. The contact conditions between the forming tools are described by the shear friction law. For the rollers and the chuck, the friction factor was 0.8. For the mandrel, which was lubricated with a mixture of Molykote HTP paste and graphite, a friction factor of 0.1 was assumed. The heat transfer conditions between the tools and the hollow billet were described by a heat transfer coefficient of 20 kW/m²K.
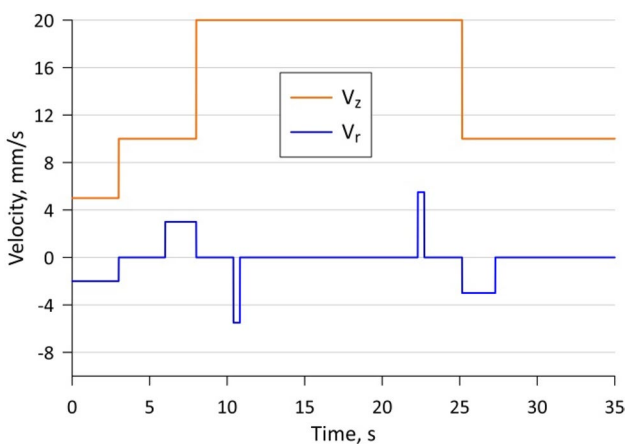
The experimental investigations were carried out using a CNC-controlled skew rolling mill, which is shown in Fig. 4. The rolling mill was equipped with an additional rotating head mounted on a hydraulic cylinder, which is shown in Fig. 4b. A mandrel (Fig. 4c) was attached to the rotating head to calibrate the inner hole of the hollow forging. To obtain the forging shown in Fig. 2, the skew rolling mill was programmed to produce a tool movement trajectory consistent with the diagram shown in Fig. 3.
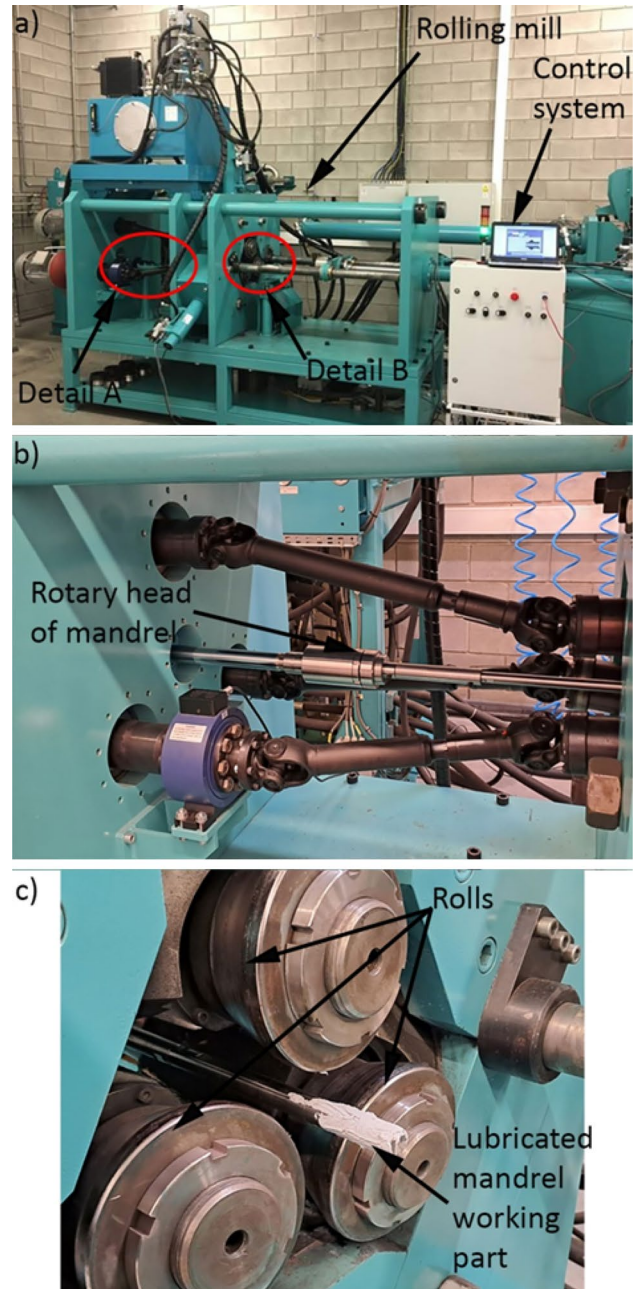

Fig. 4 Equipment used in the experimental tests: **a** CNC skew rolling mill, **b** view of detail A, **c** view of detail B

Fig. 3 Trajectory of movement of rollers and chuck

During the experimental tests, forgings were obtained and used for analysis. The skew rolling mill used was equipped with a set of pressure sensors and a torque sensor, which were used to record the energy parameters of the rolling process.

3 Results

The experimental tests carried out produced hollow railway axle forgings, which were analyzed. Examples of the forging after the rolling process are shown in Fig. 5. In the forgings obtained, it can be seen that the chuck allowance is the same length in both cases. The allowances for the rolls output of the billets are longer for the billet with a larger wall thickness. This confirms that the forging is elongated in the axial direction as a result of the mandrel blocking the radial flow of the material. Therefore, when mandrel rolling tubes with larger wall thicknesses, the length can be shortened to reduce the size of the roll's output allowance. Using disk rollers, axle forgings with good external surface quality were obtained. However, pronounced helical grooves were observed in the area of the largest forging steps (the smallest cross-sectional reduction during rolling). Shu et al. [29] rolling a mandrelless hollow shaft using disk rollers obtained helical grooves for the maximum degree of cross-sectional

reduction. The authors' study shows that using disk rollers when rolling with higher cross-sectional reductions on the mandrel, unfavorable helical grooves on the surface of forgings can be eliminated.

Based on the results of numerical simulations, the material flow pattern during the rolling of hollow railway axle forgings was analyzed. The state of strain was determined, and the factors that can negatively influence the process of skew rolling with mandrel of hollow forgings were analyzed. The shape progression of the hollow axle forging determined by the finite element method is shown in Fig. 6. The forming process starts from the chuck side towards the other end of the forging. One end of the forging is clamped in a hydraulically clamped chuck. The chuck rotates freely, and its rotation is forced by the forging clamped in it. In addition, the chuck forces the axial movement of the shaped forging at a preset velocity. Successive diameters of the forging are formed by rotating rolls that can move in a radial direction according to a preset trajectory. Based on the numerical simulation carried out, no process disturbances such as bending of the forging were found.

The numerical model built in Simufact Forming software was verified by comparing the force characteristics of the rolling process obtained from the FEM and the experiment [30]. Figure 7 shows a graph showing the radial force, axial force and torque courses obtained from the FEM and

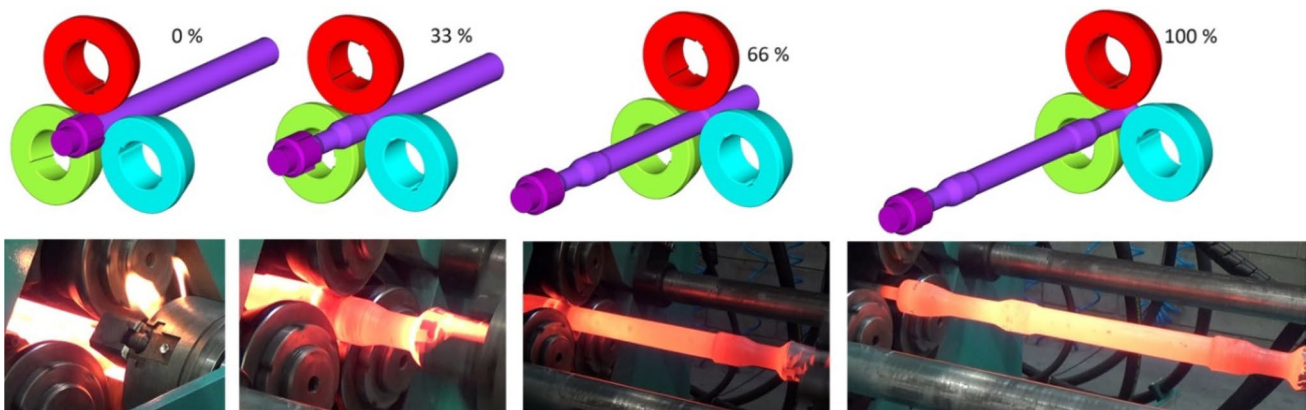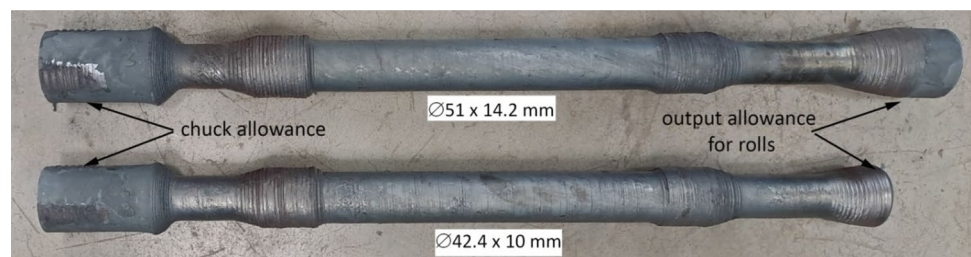**Fig. 5** General view of examples of skew rolled hollow forgings on a mandrel

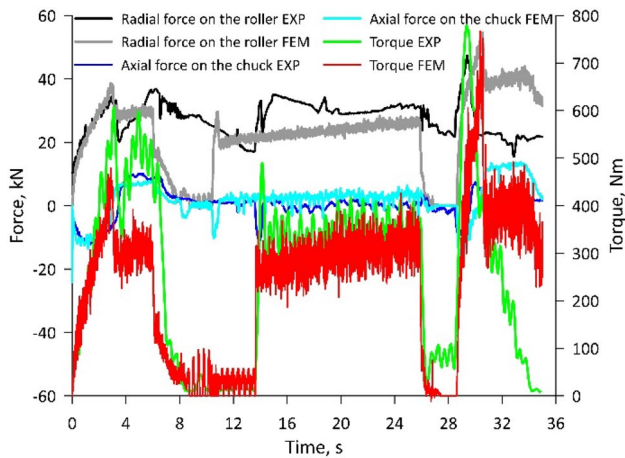**Fig. 6** Progression of the shape of a hollow railway axle forging during skew rolling

Fig. 7 Force characteristics of the hollow axle rolling process without mandrel from the billet $\varnothing 42.4 \times 10$ mm

Fig. 8 Axial cross section of railway axle forgings rolled from tubular billets: **a** $\varnothing 42.4 \times 10$ mm without mandrel, **b** $\varnothing 42.4 \times 10$ mm with mandrel, **c** $\varnothing 48.3 \times 12.5$ mm with mandrel, **d** $\varnothing 51 \times 14.2$ mm with mandrel

experiment. All force results obtained from the FEM have a very high qualitative agreement with the experimental results. The quantitative agreement was assessed using the coefficient of determination R^2. The highest value of the coefficient of determination was found in the case of the axial force, R^2 was 0.93. In the case of the torque, the value of R^2 was 0.86. The lowest value of R^2 was obtained for the radial force, at 0.63. In the case of the radial force, the greatest discrepancy between the FEM and experiment occurred during the formation of the largest forging steps. During the forming of these steps, the material was not compressed by the rollers and therefore the radial force decreased to 0 in the case of the FEM. During the rolling in the experiment, the radial force during the forming of the largest forging steps was about 20 kN. The high value of the radial force in this rolling case after despite the lack of compression of the material is due to the continuous control of the roll position by the control system, which forced the roll to be held in the set position. This phenomenon obviously does not occur during FEM calculations, which is why there is such a large discrepancy between the radial force values from FEM and experiment. The match between force characteristics from FEM and experiment is: excellent for axial force, good for torque and satisfactory for radial force. The validation of the numerical model carried out indicates a good agreement between the FEM model and the experimental conditions.

4 Analysis and discussion of results

4.1 Geometry of axle forgings

The mandrel was used to calibrate the diameter of the forging bore. Obtaining a hole with a uniform diameter
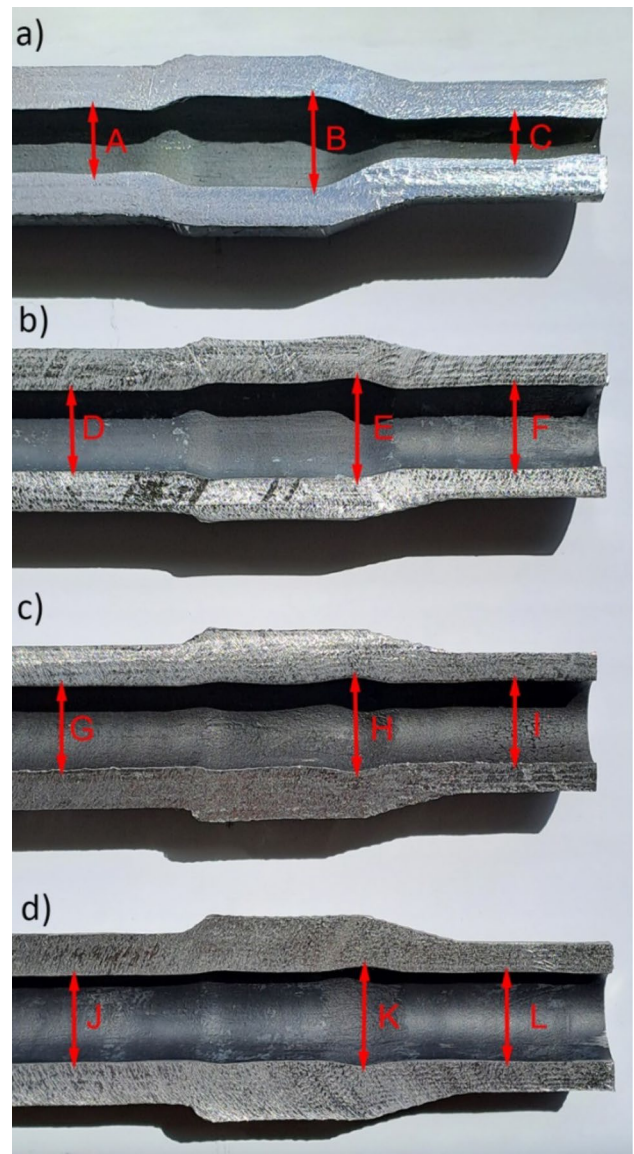
increases the accuracy of the resulting forging and minimizes the allowance removed during finishing. An axial cross-sectional view of the rolled forgings is shown in Fig. 8. In the area of the largest step of the forging, two grooves can be observed whose diameters are larger compared to the rest of the forging bore area. Similar observations were made by Wang et al. [31] analyzing the rolling accuracy of hollow products using the skew rolling method without a mandrel. Cao et al. [32] conducted a study on the process of flexible skew rolling of hollow shafts. A rolling mill with two rollers and a mandrel was used in the study. The results also indicate the problem of obtaining a hollow forging with

a diameter-homogeneous hole. Measurements were taken of the diameter of the forging bore at locations marked *A* to *L*. Measurements were carried out at these locations, where the outside diameter of the forging and thus the deformation ratio of the cross-section changes. In addition, in the case of dimensions *A*, *B*, *C*, *E*, *H,* and *K*, their location was determined at the point where this dimension reaches the highest value. A summary of the results of the measurements carried out is included in Table 1. The use of a calibrating mandrel definitely increased the dimensional accuracy of the forging bore. However, for the $\varnothing 42.4 \times 10$ mm billet, an increased hole diameter size of 23.73 ± 0.13 mm was still recorded in the area of the largest forging step. In other areas, the forging bore diameter takes on a value close to the assumed diameter of 19 mm. Increasing the billet size to $\varnothing 48.3 \times 12.5$ mm reduced the maximum size of the forging bore diameter in the area of the largest step of the forging to 21.38 ± 0.26 mm. Further increasing the billet size to $\varnothing 51 \times 14.2$ mm did not homogenize the forging bore diameter.

4.2 Strain state

The hollow railway axle forgings obtained by numerical simulation, with the distribution of effective plastic strain highlighted, are shown in Fig. 9. Comparing the results of rolling with and without a mandrel (Figs. 9a and 9b), it can be seen that higher values of plastic strain were recorded for rolling with a mandrel. This is since during mandrelless rolling, the material flows freely in the radial direction, and thus there is an increase in the wall thickness of the rolled railway axle forging. In mandrel rolling, the flow of material in the radial direction is blocked and the wall thickness at the individual forging steps is reduced. Increasing the wall thickness and outer diameter of the tubular billet leads to a marked increase in plastic strain. For the largest tubular billet (Fig. 9d), plastic deformation of the material was recorded throughout the entire volume of the forging. For all rolling cases, the largest plastic strains are located in the outer layers of the forgings that are in direct contact with the forming rolls. This is a result of the intensive flow of material in the circumferential direction due to the intense

frictional forces in this area. This distribution of strain is conducive to the formation of unfavorable residual stresses in the axle forging [33].

4.3 Thermal conditions

The temperature distribution in the rolled forgings is shown in Fig. 10. The resulting distributions are characterized by high-temperature inhomogeneity. The largest temperature reduction occurs on the drawing chuck side. As a result of the temperature decrease in this area, the ductility of the material decreases, thereby reducing the risk of wall thinning or complete forging rupture. The temperature distribution in these rolling cases will depend on the heat capacity of the billet, the amount of heat generated during plastic deformation and the amount of pressure of the shaped material on the mandrel. Comparing the cases of rolling without and with a mandrel (Fig. 10a and b), it can be seen that the use of a mandrel intensifies the temperature decrease, which is the result of heat transfer to the cooler mandrel. Increasing the wall thickness and outside diameter of the tubular billet shows a smaller temperature decrease
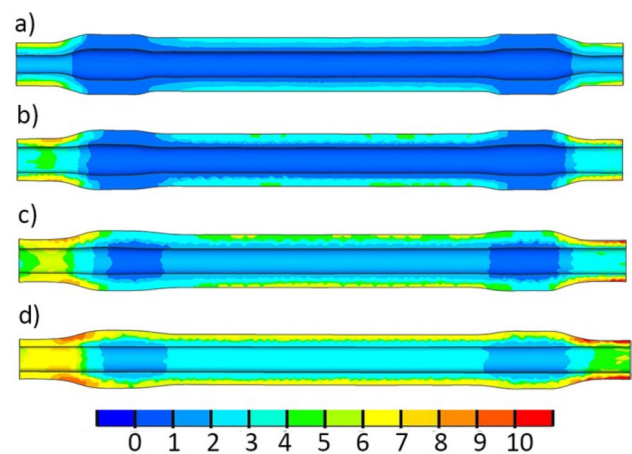

Fig. 9 Rail axle forgings with marked distribution of effective plastic strain rolled from tubular billets: **a** $\varnothing 42.4 \times 10$ mm without mandrel, **b** $\varnothing 42.4 \times 10$ mm with mandrel, **c** $\varnothing 48.3 \times 12.5$ mm with mandrel, **d** $\varnothing 51 \times 14.2$ mm with mandrel

Table 1 Summary of axle forging bore diameter measurements

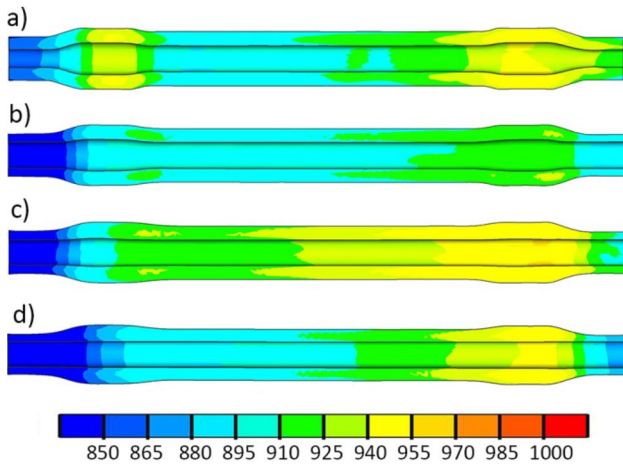| Billet	$\varnothing 42.4 \times 10$ mm without mandrel	$\varnothing 42.4 \times 10$ mm with mandrel	$\varnothing 48.3 \times 12.5$ mm with mandrel	$\varnothing 51 \times 14.2$ mm with mandrel
Dimension	A	D	G	J
Value	16.84 ± 0.23 mm	19.07 ± 0.11 mm	19.04 ± 0.15 mm	19.03 ± 0.11 mm
Dimension	B	E	H	K
Value	22.63 ± 0.13 mm	23.73 ± 0.13 mm	21.38 ± 0.26 mm	21.46 ± 0.15 mm
Dimension	C	F	I	L
Value	10.07 ± 0.38 mm	19.45 ± 0.34 mm	19.06 ± 0.32 mm	18.95 ± 0.12 mm

Fig. 10 Rail axle forgings with marked temperature distribution (°C) rolled from tubular billets: **a** $\varnothing 42.4 \times 10$ mm without mandrel, **b** $\varnothing 42.4 \times 10$ mm with mandrel, **c** $\varnothing 48.3 \times 12.5$ mm with mandrel, **d** $\varnothing 51 \times 14.2$ mm with mandrel

in the rolled forgings. The smallest temperature decrease recorded when rolling from a $\varnothing 48.3 \times 12.5$ mm billet. Increasing the wall thickness and outside diameter of the tubular billet will increase the heat capacity of the rolled material and the amount of heat generated during plastic deformation. Consequently, a smaller temperature decrease should be observed with larger tubular billet sizes. A deviation from this reasoning are the last two rolling cases, in which a larger temperature decrease occurred for the billet with the largest size. Consequently, the value of the pressure of the rolled material on the mandrel can have a decisive influence on the temperature distribution.

An example of a thermogram of a forging after rolling from a $\varnothing 48.3 \times 12.5$ mm billet with a mandrel is shown
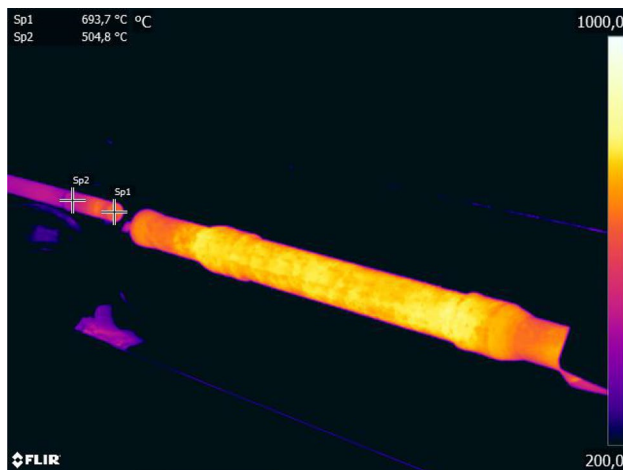
in Fig. 11. The temperature on the surface of the forging after rolling is less than 1000 °C. A clear decrease in temperature can be observed at the extremes of the forging. The greatest temperature decrease is observed in the area of the extreme step of the forging on the drawing chuck side. The thermogram obtained during the experiment is in good agreement with the thermogram obtained from the FE analysis. The temperature of the mandrel after rolling was also recorded in the thermogram shown. Before rolling, the mandrel was at ambient temperature. During rolling, the temperature on the surface of the mandrel increased to about 700 °C. This is a very unfavorable phenomenon, as it will significantly affect the lifetime of the mandrel. For industrial applications, the mandrel should be cooled intensively during rolling or immediately after the rolling of the forging is completed.

4.4 Force parameters

Figures 12–14 summarize the force parameters of the rolling process of hollow railway axle forgings from billets of different initial sizes. The force parameter distributions shown were recorded during experimental tests of the rolling process. The distribution of the torque measured on the forming roll (Fig. 12) shows that increasing the wall thickness of the billet increases this parameter. Considering the case of rolling with and without a mandrel, it can be observed that the use of a mandrel to calibrate the internal hole causes an increase in torque.

The distribution of the axial force on the drawing chuck is shown in Fig. 13. From the distribution shown, it can be seen that the axial force increases as the wall thickness of the tubular billet increases. Comparing the case of rolling from the $\varnothing 42.4 \times 10$ mm billet with and without a mandrel,
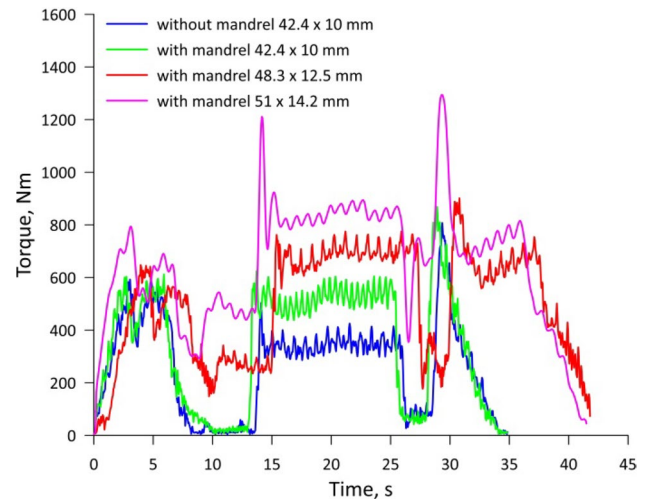

Fig. 11 Thermogram of **a** rolled axle forging from **a** $\varnothing 48.3 \times 12.5$ mm billet with mandrel

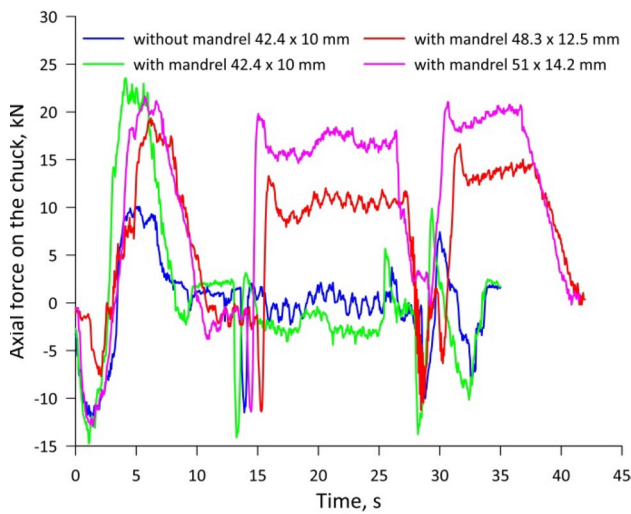

Fig. 12 Torque distribution on the roll

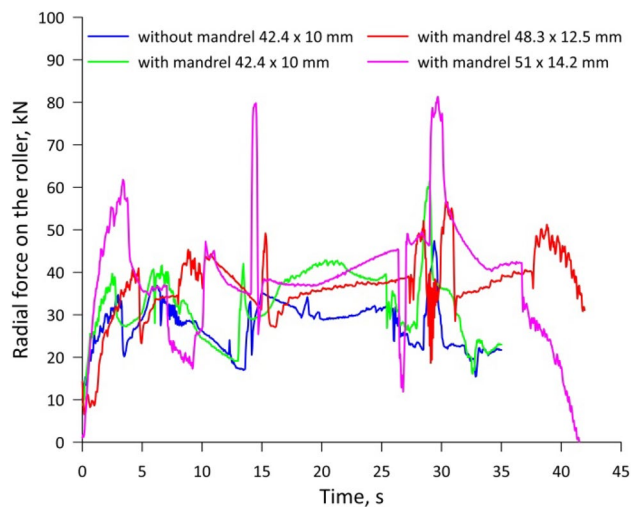**Fig. 13** Distribution of axial force on the drawing chuck

Fig. 14 Distribution of radial force on the roll

it was observed that when rolling the center step of the axle forging, a higher axial force occurs when rolling without a mandrel. This situation is probably due to the free flow
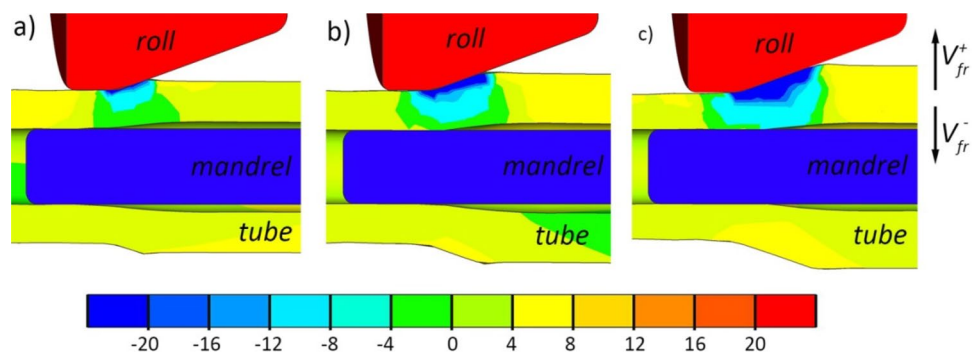
of the material in the radial direction, which results in an increase in the wall thickness of the forging. This is because that with greater forging wall thickness, there is an increase in the resistance to deformation of the material in the axial direction, which induces the material to flow in the radial direction.

The distribution of the radial force on the roll during rolling is shown in Fig. 14. The course of the radial force is not as stable as in the case of the axial force and torque, where it is clear at what time each step of the forging is rolled. The instability of the radial force may be the result of disturbances due to changes in the position of the rolls during rolling, resulting from the rolls striving to maintain a preset position. Nevertheless, it can be observed that the lowest value of the radial force during rolling of the central step of the forging occurs during rolling without a mandrel. On the other hand, the highest values occur when rolling with mandrel from billets $\varnothing 42.4 \times 10$ mm and $\varnothing 51 \times 14.2$ mm. In the first case, with a smaller tube wall thickness the material can be pressed intensively into the mandrel, resulting in an increase in radial force and contact pressure on the mandrel. In the second case, the greater wall thickness of the tubular billet will also result in an increase in plastic deformation resistance, which will translate into higher radial force values. The increased radial force values in these two rolling cases will have a significant effect on the increase in contact pressure between the rolled material and the mandrel. The increase in contact pressure between the rolled material and mandrel will result in intensive cooling of the rolled forging and, thus, greater heating of the mandrel, as confirmed by the temperature distribution of the axis forgings shown in Fig. 10.

4.5 Material flow pattern

The pattern of material flow during the rolling of the middle stage of the forging ($\varnothing 37.5$ mm) in the radial direction in the same direction as the roll's velocity V_r (Fig. 1) is shown in Fig. 15. It can be seen from the presented distribution that an increase in the external diameter of the tube and its thickness causes an increase in the material flow velocity

Fig. 15 Distribution of material flow velocity V_{fr} in mm/s in radial direction: **a** $\varnothing 42.4 \times 10$ mm with mandrel, **b** $\varnothing 48.3 \times 12.5$ mm with mandrel, **c** $\varnothing 51 \times 14.2$ mm with mandrel

in the mandrel direction. For all the rolling cases analyzed, significantly more intensive flow of material in the radial direction occurs in the area immediately adjacent to the forming roll. In the area near the mandrel, the material flow velocities are considerably lower. In summary, the material flow velocity varies along the radius of the formed tube from maximum velocity at the largest tube radius to minimum velocity at the smallest radius. An increase in the material flow velocity in the radial direction causes the tube to contact the mandrel over a longer distance. The greatest problems with material detachment from the mandrel occur in the area of the largest step of the $\varnothing 43$ mm diameter forging. It was, therefore, decided to analyze this rolling stage in more detail.

Figure 16 shows the successive stages of rolling a step of a forging with a diameter of $\varnothing 43$ mm from a tube with initial dimensions of $\varnothing 48.3 \times 12.5$ mm. In stage 1 of rolling, it can be seen that the material flows towards the mandrel. In stage 2, in which the roll moves outwards to achieve the assumed diameter of the largest step of the forging, a lack of flow of material towards the mandrel is observed. In stage 3, a gap can be observed due to the outward movement of the roll. In stage 4, as the roll moves towards the mandrel, an increase in the intensity of material flow towards the mandrel can be observed. In summary, it can, therefore, be concluded that the improper forming of the forging bore is the result of a change in the spacing of the forming rolls for a change in the diameter of the rolled forging.

4.6 New concept for rolling hollow railway axles on a mandrel

Based on the material flow analysis shown in Fig. 16, a new concept for the rolling of hollow railway axles on a mandrel shown in Fig. 17 was proposed. The new rolling method consists of a two-stage forming of the hollow railway axle. In the first pass, the outside diameter of the billet is reduced

on the mandrel to a maximum rail axle forging diameter of 43 mm. In this stage of rolling, the forming rolls do not change their position to obtain an internal hole with a constant diameter. In the second pass, the final shape of the railway axle forging is rolled on the mandrel.

To verify the new rolling concept, experimental tests were carried out under the conditions described in Chapter 2. The resulting hollow railway axle forging rolled in two stages is shown in Fig. 18. The application of two-stage rolling technology made it possible to obtain a hollow railway axle forging with better internal bore parameters. The two-stage rolling did not eliminate material detachment from the mandrel in the area of the largest step of the forging. The largest dimension of the forging bore in this rolling case is $\varnothing 20.34$ mm. Compared to the single-pass rolled forging shown in Fig. 8d, the two-pass rolled forging has a more uniform hole diameter. The use of two-pass rolling has made it possible to reduce the maximum size of the grooves formed in the area of the step of the largest diameter forging by 1.12 mm, compared with one-pass rolling. The results obtained will significantly reduce the amount of allowance needed to be removed by machining. In the case of rolling a 1:1 scale hollow axle forging, this will reduce the allowance on diameter by 5.6 mm.

4.7 Gap between the bore diameter and the mandrel diameter

To summarize the results obtained, the gap c between the bore diameter of the forging and the diameter of the mandrel was measured. After the tests, it was found that there were two gaps in the area of the largest step of the forging (Fig. 8. and Fig. 18.). In the measurements carried out, the focus was on the gap with the larger size in each case, as this determines the accuracy of the forging. The results of the measurements carried out are summarized in the form of the graph shown in Fig. 19. The largest gap c
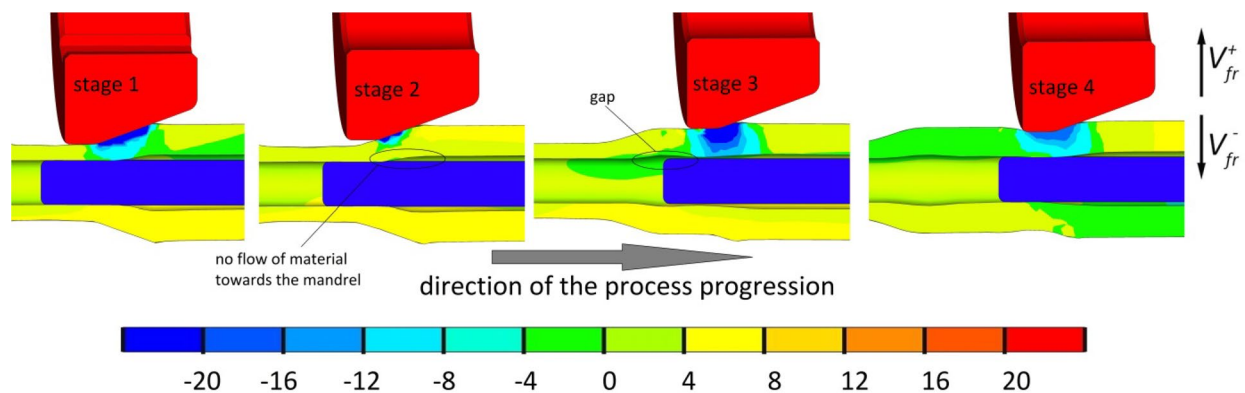

Fig. 16 Distribution of material flow velocity V_{fr} in mm/s in the radial direction during the rolling of a step forging with a diameter of $\varnothing 43$ mm from a tube $\varnothing 48.3 \times 12.5$ mm with a mandrel
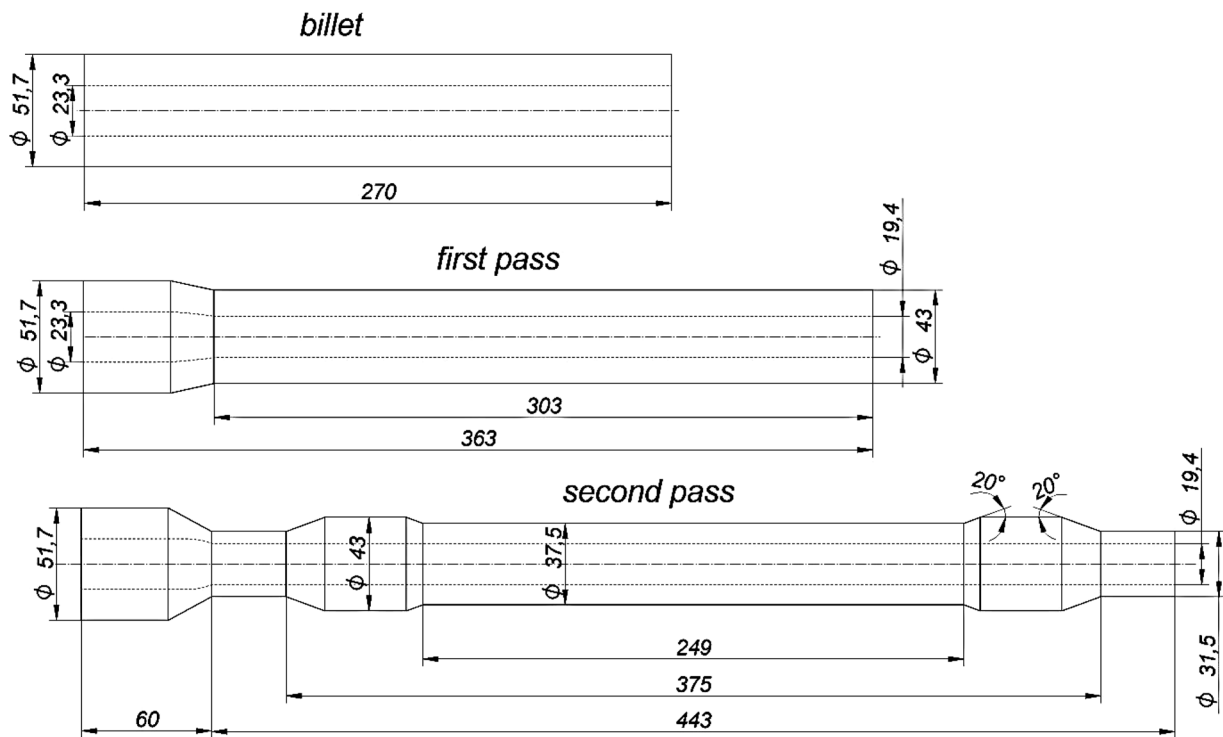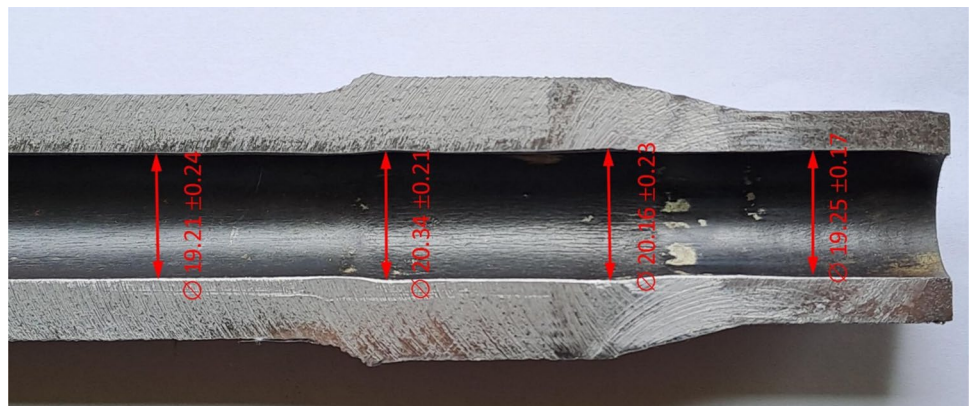
Fig. 17 Schematic of a two-stage rolling process for **a** hollow railway axle forging

Fig. 18 Axial section of a railway axle forging rolled in two passes from a tubular billet $\varnothing 51 \times 14.2$ mm with mandrel

between the axle bore, and the mandrel was recorded for the case of rolling from a billet of $\varnothing 42.4 \times 10$ mm and is 2.37 ± 0.07. The smallest gap c was recorded for the case of rolling from a billet of $\varnothing 51 \times 14.2$ mm in two passes and is 0.67 ± 0.11. By modifying the rolling system, the size of the gap c is reduced by 71.7%. An increase in the billet size above $\varnothing 48.3 \times 12.5$ mm did not result in a clear reduction in the gap c formed between the axle bore and the mandrel, but even a slight increase. A definite reduction in the gap c between the axle bore and mandrel occurred in the case of two-stage rolling. Increasing the billet dimensions from $\varnothing 42.4 \times 10$ mm to $\varnothing 48.3 \times 12.5$ mm reduced the gap c by

49.8%. Rolling the billet $\varnothing 51 \times 14.2$ mm in two passes compared to rolling in one pass reduced the gap c by 45.5%.

4.8 Microstructure and mechanical properties

Axle forgings were subjected to hardness tests to measure mechanical properties. The forgings for testing were in the as-rolled condition and free cooling in air. The results of the hardness measurements using the Vickers HV10 method are shown as a graph in Fig. 20. The hardness measurements were taken at 10 measurement points distributed over the entire thickness of the forging wall. The hardness distribution for all cases analyzed is
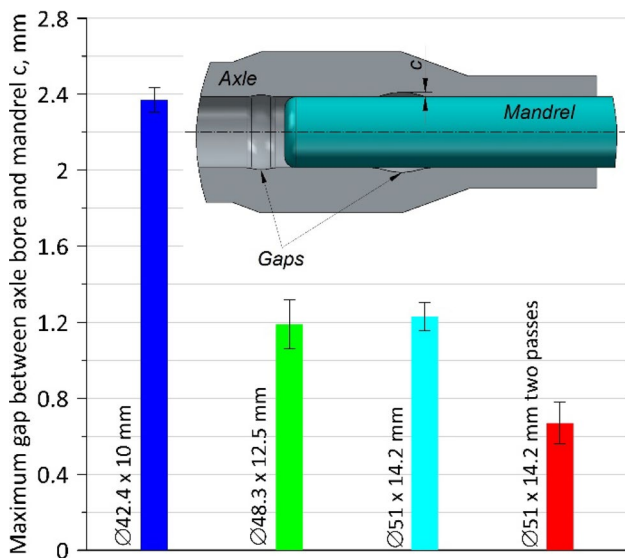
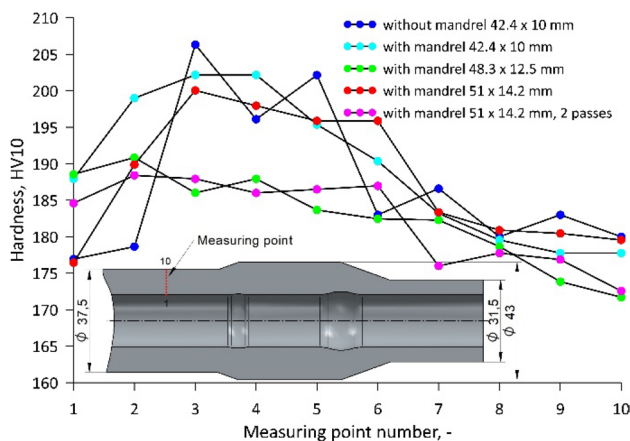**Fig. 19** Maximum gap between axle bore and mandrel *c* for the analyzed rolling cases

Fig. 20 Distribution of hardness HV10 over wall thickness

neighborhood of points 3 and 4. In the inner area of the forging wall (point 1), the hardness takes on intermediate values. In the case of forgings rolled from billets $\varnothing 48.3 \times 12.5$ mm and $\varnothing 51 \times 14.2$ mm in two passes, the hardness takes on significantly smaller values in the middle of the wall thickness than in the other rolling cases. The results obtained indicate inhomogeneity of hardness across the forging wall thickness. Table 2 summarizes the average hardness values along the wall thickness, together with the standard deviation values from the average value. The highest average hardness value of 189.5 HV10 was obtained for rolling from a billet of $\varnothing 48.3 \times 12.5$ mm. The smallest average hardness value of 182.4 HV10 occurred when rolling from a billet of $\varnothing 51 \times 14.2$ mm in two passes. The scatter in hardness along the wall thickness was measured by standard deviation. The measurements show that the greatest homogeneity of hardness (smallest standard deviation $s = 5.9$) occurs when rolling from a billet of $\varnothing 51 \times 14.2$ mm in two passes. On the other hand, the smallest homogeneity of hardness (largest standard deviation $s = 10.5$) occurs when rolling from billet $\varnothing 42.4 \times 10$ mm without a mandrel.

The axle forgings were subjected to metallographic testing to estimate the microstructure. The forgings for metallographic testing were in identical condition to those for hardness testing. Observations of the microstructure were carried out after grinding and polishing of the metallographic scrap and etching with nital 2% reagent. The metallographic specimens were taken from the same part of the axle forging where the hardness measurement was carried out. Figure 21 shows, in graph form, the average grain size of the axle microstructure for the rolling cases analyzed. The largest grain size of 10.25 ± 1.03 μm occurred in the case of rolling without a mandrel. On the other hand, the finest grain size of 7.59 ± 0.96 was possessed by the axle forgings rolled from the billet $\varnothing 51 \times 14.2$ mm in two passes. Forgings rolled from the $\varnothing 48.3 \times 12.5$ mm and $\varnothing 51 \times 14.2$ mm in two passes have similar microstructure grain sizes. Furthermore, in these two cases the scatter of the measurement error is the smallest, indicating a rather high homogeneity of grain size compared to the other cases. It can, therefore,

similar. The smallest hardness values were recorded in the outer area of the forging wall (point 10). The highest hardness, on the other hand, is found in the area located approximately in the middle of the wall thickness in the

Table 2 Average hardness values and hardness scatter

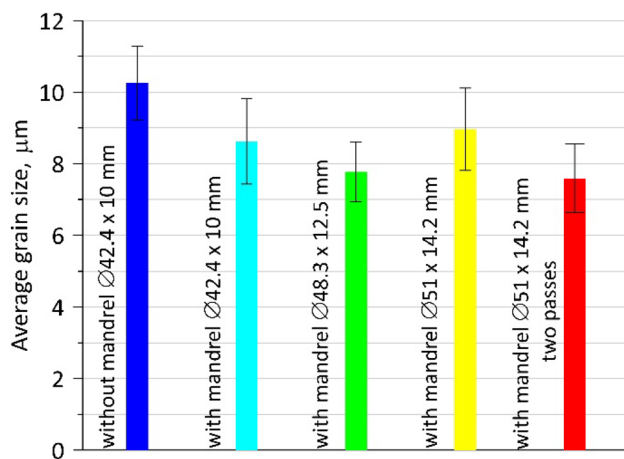| Billet	$\varnothing 42.4 \times 10$ mm without mandrel	$\varnothing 42.4 \times 10$ mm with mandrel	$\varnothing 48.3 \times 12.5$ mm with mandrel	$\varnothing 51 \times 14.2$ mm with mandrel	$\varnothing 51 \times 14.2$ mm with mandrel 2 passes
Average hardness, HV10	187.3	189.5	182.6	188.0	182.4
Standard deviation s	10.5	9.8	6.3	8.9	5.9

Fig. 21 Average grain size of the microstructure of railway axle forgings

be concluded that the homogeneity of the grain size of the microstructure is reflected in a homogeneous hardness distribution along the wall of the axle forgings (Fig. 20).

Figure 22 shows an example of the microstructure of a forging with the largest and smallest grain size. In both cases, the microstructure is ferritic-perlite. In the microstructure of the rolled axle without mandrel, the perlite grains have a less regular shape compared to the perlite grains in the microstructure of the rolled axle from the billet $\varnothing 51 \times 14.2$ mm in two passes. Thus,

the distribution of perlite grains in the microstructure of the two-pass rolled axle is more uniform than in the case of the mandrelless rolled axle. Regardless of grain size, grain shape, and grain distribution, both structures are typical of the microstructure of S355J steel in the state after normalization [34]. In the analyzed area of the microstructure, the typical characteristics of the microstructure after overheating with too little plastic deformation, which is typical of skew rolling processes, were not observed [35].

5 Conclusions

A study was carried out on the three-roll skew rolling (TRSR) process of hollow railway axle forgings. Based on the numerical and experimental studies performed, the following final conclusions were obtained:

- The TRSR method allows the manufacture of hollow railway axle forgings on a mandrel.
- The use of a calibrating mandrel increases the uniformity of the bore diameter of the forging.
- The rolling of hollow forgings with a mandrel should be carried out from tubular billets with larger dimensions, i.e., outside diameter and wall thickness.
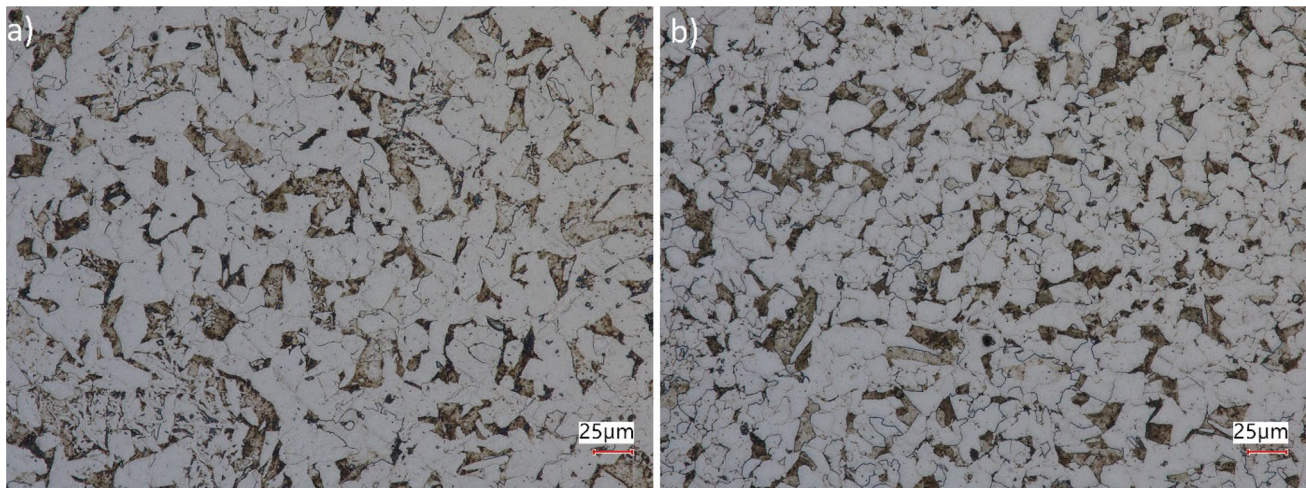

Fig. 22 Microstructure of the axle forging in the analysis area: **a** $\varnothing 42.4 \times 10$ mm.without mandrel, **b** $\varnothing 51 \times 14.2$ mm with mandrel 2 passes

- Increasing the spacing of the forming rolls during rolling is responsible for the increase in the diameter of the forging bore.
- The two-stage TRSR method increases the uniformity of the forging bore diameter.

The geometry of the rollers used in the TRSR process can have a significant impact on the bore accuracy of hollow forgings, including railway axles. Future studies would need to consider the effect of the taper angle of the forming roll. Another issue is the possibility of using rolls of a different shape, e.g., with a radius in the shaping part of the roll.

Data availability The datasets and material generated and/or analyzed during current study are available from the corresponding author on reasonable request.

Declarations

Conflict of interest The authors have no conflicts of interest/competing interests to declare that are relevant to the content of this article.

Ethical approval The article follows the guidelines of the Committee on Publications Ethics (COPE) and involves no studies on human or animal subjects.

Consent to participate Applicable.

Consent to publish Applicable.

References

1. Pomykała A, Engelhardt J. Concepts of construction of high-speed rail in Poland in context to the European high-speed rail networks. Socio-Econ Plan Sci. 2023;85: 101421. https://doi.org/10.1016/j.seps.2022.101421.

2. Mindur L, Mindur M. The development of high-speed rail in the Federal Republic of Germany between 2002–2020. Sci J Sil Univ Technol Ser Transp. 2022;117:151–74.

3. Fu ZH, Yang BJ, Shan ML, Li T, Zhu ZY, Ma CP, Zhang X, Gou WZR, Hydrogen GW. embrittlement behavior of SUS301L-MT stainless steel laser-arc hybrid welded joint localized zones. Corros Sci. 2020;164:108337.

4. Giętka T, Ciechacki K. Modeling of railway wheels made of austempered ductile iron. Arch Metall Mater. 2016;61(4):1833–8. https://doi.org/10.1515/amm-2016-0296.

5. Kowalski S. Selected problems in the exploitation of wheel sets in rail vehicles. J Mach Constr Maint. 2017;105(2):109–16.

6. Smith RA. Fatigue of railway axles: A classic problem revisited. In: Fuentes M, Elices M, Martín-Meizoso A, Martínez-Esnaola JM, editors. Fracture Mechanics: Applications and Challenges. San Sebastián: Elsevier; 2000. p. 173–81.

7. Shi J, Zhao B, He T, Tu L, Lu X, Xu H. Tribology and dynamic characteristics of textured journal-thrust coupled bearing considering thermal and pressure coupled effects. Tribol Int. 2023;180: 108292. https://doi.org/10.1016/j.triboint.2023.108292.

8. Ognjanovic M, Simonovic A, Ristivojevic M, Lazovic T. Research of rail traction shafts and axles fractures towards impact of service conditions and fatigue damage accumulation. Eng Fail Anal. 2010;17:1560–71. https://doi.org/10.1016/j.engfailanal.2010.06.007.

9. Luo Y, Wang H, Li C, Ren X, Wu S. Fatigue strength assessment of high-speed railway axle EA4T steel with foreign object damage. Eng Fail Anal. 2022;133: 105961. https://doi.org/10.1016/j.engfailanal.2021.105961.

10. Lin LF, Wang BY, Liu JP, Zheng ZH, Zhu CB. An application exploration of flexible skew rolling a rail car axle. IOP Conf Ser Mater Sci Eng. 2022;1270: 012082. https://doi.org/10.1088/1757-899X/1270/1/012082.

11. Mistry PJ, Johnson MS. Lightweighting of railway axles for the reduction of unsprung mass and track access charges. Proc Inst Mech Eng F J Rail Rapid Transit. 2020;234(9):958–68. https://doi.org/10.1177/0954409719877774.

12. Son S, Jung H, Choi S. Study on design of railway hollow axle. Trans Korean Soc Automot Eng. 2014;22(4):46–54. https://doi.org/10.7467/KSAE.2014.22.4.046.

13. Huang H, Yao Y, Liang C, Ye Y. Experimental study on cyclic performance of steel-hollow core partially encased composite spliced frame beam. Soil Dyn Earthq Eng. 2022;163: 107499. https://doi.org/10.1016/j.soildyn.2022.107499.

14. Xu Y, Zhang Y, Zhuang X, Cao Z, Lu Y, Zhao Z. Numerical modeling and anvil design of high-speed forging process for railway axles. Int J Mater Form. 2021;14:813–32. https://doi.org/10.1007/s12289-020-01590-9.

15. Gronostajski Z, Pater Z, Madej L, Gontarz A, Lisiecki L, Łukaszek-Sołek A, et al. Recent development trends in metal forming. Arch Civ Mech Eng. 2019;19(3):898–941. https://doi.org/10.1016/j.acme.2019.04.005.

16. Campi F, Mandolini M, Favi C, Checcacci E, Germani M. An analytical cost estimation model for the design of axisymmetric components with open-die forging technology. Int J Adv Manuf Technol. 2020;110:1869–92. https://doi.org/10.1007/s00170-020-05948-w.

17. Biermann D, Bleicher F, Heisel U, Klocke F, Möhring HC, Shih A. Deep hole drilling. CIRP Ann Manuf Technol. 2018;67:673–94. https://doi.org/10.1016/j.cirp.2018.05.007.

18. Biermann D, Kirschner M, Eberhardt D. A novel method for chip formation analyses in deep hole drilling with small diameters. Prod Eng Res Devel. 2014;8:491–7. https://doi.org/10.1007/s11740-014-0566-7.

19. Mistry PJ, Johnson MS, McRobie CA, Jones IA. Design of a lightweight multifunctional composite railway axle utilising coaxial skins. J Compos Sci. 2021;5(3):77. https://doi.org/10.3390/jcs5030077.

20. Johnson MS, Evans R, Mistry P, Li S, Bruni S, Bernasconi A, Cervello S. Structural analysis for the design of a lightweight composite railway axle. Compos Struct. 2022;290: 115544. https://doi.org/10.1016/j.compstruct.2022.115544.

21. Mistry PJ, Johnson MS, Li S, Bruni S, Bernasconi A. Parametric sizing study for the design of a lightweight composite railway axle. Compos Struct. 2021;267: 113851. https://doi.org/10.1016/j.compstruct.2021.113851.

22. Carra G, Formaggioni D, Johnson MS, Mistry PJ, Bernasconi A, Bruni S. Optimization of a filament wound hybrid metal composite railway axle design concept. Appl Sci Eng Prog. 2022;15(2):5791.

23. Pater Z, Tomczak J, Bulzak T, Wójcik Ł. Conception of a three roll cross rolling process of hollow rail axles. ISIJ Int. 2021;61(3):895–901. https://doi.org/10.2355/isijinternational.ISIJINT-2020-530.

24. Nwe T, Pimsarn M. Railway axle and wheel assembly press-fitting force characteristics and holding torque capacity. Appl Sci. 2021;11(19):8862. https://doi.org/10.3390/app11198862.

25. Shen J, Wang B, Yang C, Zhou J, Cao X. Theoretical study and prediction of the inner hole reduction and critical mandrel diameter in cross wedge rolling of hollow shaft. J Mater Process Tech. 2021;294: 117140. https://doi.org/10.1016/j.jmatprotec.2021.117140.

26. Shu C, Zhang S, Bidare P, Essa K, Abdel-Wahab A, Shu X, Pater Z, Bartnicki J. Microstructure evolution of three-roll skew-rolling formed hollow axles with uniform wall thickness. Int J Adv Manuf Technol. 2022;121:4069–85. https://doi.org/10.1007/s00170-022-09583-5.

27. Pater Z. A comparative analysis of forming railway axles in 3- and 4-roll rolling mills. Materials. 2020;13(14):3084. https://doi.org/10.3390/ma13143084.

28. Yu B, Chen Z, Wang P, Song X. A comparative study on the mechanical behavior of S355J2 steel repair-welded joints. J Constr Steel Res. 2023;205: 107878. https://doi.org/10.1016/j.jcsr.2023.107878.

29. Shu X, Zhang S, Shu C, Wang J, Ye C, Xia Y, Essa K, Pater Z. Research and prospect of flexible forming theory and technology of hollow shaft by three-roll skew rolling. J Adv Manuf Technol. 2022;123:689–707. https://doi.org/10.1007/s00170-022-10242-y.

30. Yang Y, Lin B, Zhang W. Experimental and numerical investigation of an arch-beam joint for an arch bridge. Archiv Civ Mech Eng. 2023;23:101. https://doi.org/10.1007/s43452-023-00645-3.

31. Wang J, Shu X, Ye C, Li Z, Li S, Xu H, Wang Y, Deng Y, Chen Q. Study on forming quality of three-roll skew rolling hollow axle. J Adv Manuf Technol. 2023;128:1089–100. https://doi.org/10.1007/s00170-023-11893-1.

32. Cao X, Wang B, Guo W, Ju Z. A new method of manufacturing hollow shafts via flexible skew rolling. J Phys Conf Ser. 2021;2101: 012010. https://doi.org/10.1088/1742-6596/2101/1/0120.

33. Zhu Q, Chen J, Gou G, Chen H, Li P. Ameliorated longitudinal critically refracted—Attenuation velocity method for welding residual stress measurement. J Mater Process Tech. 2017;246:267–75. https://doi.org/10.1016/j.jmatprotec.2017.03.022.

34. Pańcikiewicz K, Tuz L. Microstructure and mechanical properties of S355 structural steel multirun tee-joint made by robot motioned MAG method. Weld Tech Rev. 2013;85:34–40.

35. Pater Z, Tomczak J, Bulzak T, Walczuk-Gągała P. Numerical and experimental study on forming preforms in a CNC skew rolling mill. Arch Civ Mech Eng. 2022;22:54. https://doi.org/10.1007/s43452-022-00373-0.